

*Math. Model. Nat. Phenom.*  
Vol. 12, No. 4, 2017, pp. 15–29  
DOI: 10.1051/mmnp/201712403

# Limb Movement in Dynamic Situations Based on Generalized Cognitive Maps

J. A. Villacorta-Atienza<sup>1\*</sup>, C. Calvo<sup>1\*</sup>, S. Lobov<sup>2</sup>, V. A. Makarov<sup>1,2\*\*</sup>

<sup>1</sup>Instituto de Matemática Interdisciplinar, Dept. de Matemática Aplicada,  
Universidad Complutense de Madrid, Avda. Complutense s/n, 28040 Madrid, Spain

<sup>2</sup>Lobachevsky State University of Nizhny Novgorod, Gagarin Ave. 23, 603950 Nizhny Novgorod, Russia

**Abstract.** The fundamental bases of how our brain solves different tasks of object manipulation remain largely unknown. Here we consider the problem of the limb movement in dynamic situations on an abstract cognitive level and propose a novel approach relying on: i) transformation of the problem from the limb workspace to the so-called hand-space, and ii) construction of a generalized cognitive map (GCM) in the hand-space. The GCM provides a trajectory that can be followed by the limb, which ensures an efficient collision-free movement and target catching in the workspace. Our numerical simulations confirm the approach feasibility but also reveal the problem complexity. We then validate the GCM-based solutions in real-life scenarios. We show that a GCM-equipped humanoid robot can catch a fly ball in a similar way as a human subject does. The static nature of the GCMs enables learning and automation of sophisticated cognitive behaviors exhibited by humans.

**Keywords and phrases:** cognitive models, robot manipulators, internal representations, cognitive maps

**Mathematics Subject Classification:** 93C85, 68T40, 34G20

## 1. Introduction

Sensory-motor abilities routinely exhibited by humans may appear simple at the first glance. However, many of these ordinary skills as, e.g., catching a moving ball by hand, eventually require forecasting future states of the environment (not only of the ball) and matching them with the body movements accessible to the subject. At the time being the intrinsic complexity of this problem impedes the robots to imitate smoothly even basic human motor abilities. In real-life scenarios the limb manipulation cannot be driven purely programmatically, but requires support on an abstract cognitive level. The mathematical description of this level is an open problem in cognitive robotics.

Recent experimental and computational evidence suggests that the cognitive processes behind the sensory-motor transformation rely on an internal representation of the body and the environment [1–5]. The emergent internal (or mental) model of the world can be used to perform rehearsal of movements to master skills, which is especially useful in dynamic situations, i.e., when the external world changes

---

\*These authors contributed equally.

\*\*Corresponding author. E-mail: vmakarov@ucm.es

in time. Then the subject before extending a limb towards a moving object has to decide consciously or subconsciously how the task can be fulfilled. The direct naive solution – “stretch out your hand towards the object” – may fail. Indeed, the limb can either miss the moving object or even bump against static or moving obstacles. In this situation, an internal model may help evaluating the fitness of different motor responses and thus selecting the best strategy to accomplish the goal [6, 7]. There are also attempts to use the neural activity involved in these processes in devices providing disabled persons with control of artificial limbs or computers [8, 9].

One of the most fruitful approaches to the problem of movement of artificial limbs employs theory of dynamical systems for modeling the limb–environment interaction. In particular, the use of potential fields and modeling of a perturbed damped oscillator were proposed as a tool to determine the movement primitives [10, 11]. Another approach to the collision avoidance simulates an elastic strip that enables dynamic selection among different but homotopic paths [12]. In Ref. [13] the authors proposed a technique to modulate the original dynamics of the limb controller, which increases the robot reactivity in the face of unexpected changes in the environment. Although these approaches were intended to resolve both static and dynamic situations, in dynamic scenarios they are reduced to a local adaptation to changes in the environment. Then the local decision-making may be ineffective in situations requiring a global approach, e.g., in the presence of several moving obstacles. Another technique is based on learning programmatically the human behavior from demonstration. It was shown that the robot can make a global prediction and catch an irregular object in flight [14].

Despite significant advances in the controlling manipulators, the abstract cognitive dimension of the problem has been much less addressed in the literature. Growing experimental evidence suggests that animals use *cognitive maps* (CMs) for planning and executing movements (see, e.g., [3]). A CM is an abstraction of the environment that structures relevant “geographical” information such as the position and size of objects, the subject location, etc. Besides, it also includes rules on how to trace trajectories to a target that can be followed by the subject. However, the CM concept works well in static situations only. Recently, we proposed a theory of *generalized cognitive maps* (GCMs) that describes functional mechanisms supporting the cognition of dynamic situations [15–17]. Briefly, a GCM is built by a wave propagating in a neural network. The wave extracts the relevant *spatiotemporal* events from the environment and projects them into a purely static map. Thus, the time dimension is “compacted” and we get a static internal representation of a dynamic situation.

The GCMs have been originally developed for agents with rigid body, i.e., without internal degrees of freedom [18]. The significant spatial extension and changing geometry of a limb bring additional degree of complexity, which invalidates the direct application of the GCM concept to manipulators. The common strategy to remedy this complexity is to pass the problem from the workspace (i.e., the real space where a limb actuates) to a new space, called the configuration or task space [19]. The configuration space represents the set of all possible configurations of a manipulator and usually it is equivalent to the space of joint angles. Then it serves as a natural framework for solving the direct and inverse kinematic problems. We, however, depart from this approach.

Here we propose a holistic model of a limb embedded in a dynamic situation. The model exploits the GCM concept and thus provides the limb with cognitive abilities at an abstract global level. To deal with the internal degrees of freedom we adopt a transformation to a configuration space. However, this space, called the hand-space, is isometric to the workspace. It allows representing the limb as a single point, but the price to pay is the extension of the obstacles, e.g., a point-like obstacle is mapped to a curve. Nevertheless, the latter makes no problem for building a GCM in the hand-space. The imposed equivalence between the work- and hand- spaces enables direct motor implementation of the trajectories found in the hand-space, i.e., no inverse transformation to the workspace is required. Thus, we develop a consistent and efficient theoretical framework supporting cognitive manipulation in artificial agents.

## 2. Holistic model of cognitive limb embedded in dynamic situations

As we mentioned in the Introduction the original concept of generalized cognitive maps has been developed for rigid agents reducible to a point in the internal neuronal space [15]. Now we will show how this concept can be extended to manipulators with several joints working in dynamic situations.

### 2.1. Limb configuration and geometric constraints in workspace

Figure 1A illustrates a two-joint manipulator, an articulated upper-limb, which can move in a workspace,  $\mathcal{W} \subset \mathbb{R}^2$ , given on the two-dimensional plane  $(x_1, x_2)$ . The limb shoulder is fixed at the plane origin by a revolving joint. The shoulder is joined to an articulated elbow located at  $\mathbf{x}_e \in \mathbb{R}^2$  by a rigid segment of length  $\rho$ . A forearm of length  $l$  joins the elbow with a hand located at  $\mathbf{x}_h \in \mathbb{R}^2$ . To generalize the further calculations we rescale the spatial coordinates to arbitrary units in such a way that the length of the forearm is  $l = 1$  a.u. Thus, in what follows all distances are given in the units rescaled to the forearm length. We then restrict the workspace to  $\mathcal{W} = \bar{\mathcal{B}}_{\rho+1}(\mathbf{0})$ , where  $\bar{\mathcal{B}}_{\rho+1}(\mathbf{0})$  is a closed disk of radius  $\rho + 1$  centered at the origin.

The shoulder and elbow joints can freely rotate, thus changing the geometrical configuration of the limb and, consequently, the hand position. Then our goal is to catch by the hand a target and simultaneously avoid collisions with obstacles. In general, the target and obstacles can move and have arbitrary shape. We thus aim at a holistic model of the limb that would allow solving this problem efficiently.

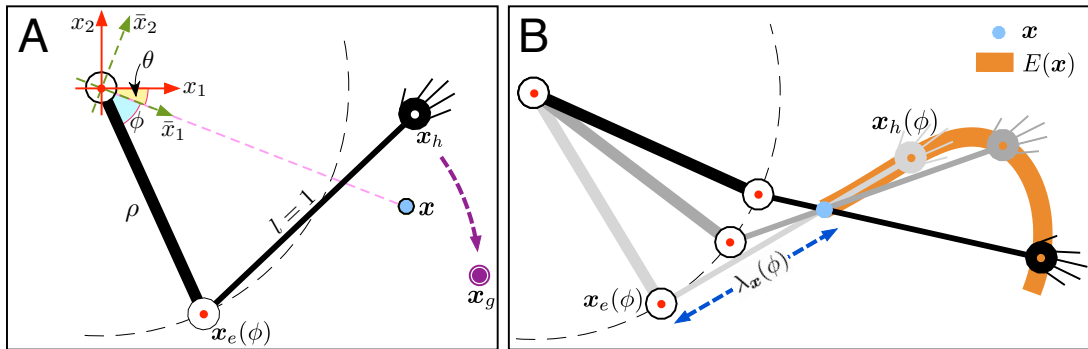


FIGURE 1. Sketch of a two-joint manipulator (an upper limb) in workspace  $\mathcal{W}$  and a constraint imposed by an obstacle on the limb movements. A) The shoulder is fixed in the origin. Upper arm and forearm have lengths  $\rho$  and  $l = 1$  a.u., respectively. The upper arm forms the angle  $\phi$  with the direction to a point-like obstacle located at  $\mathbf{x}$  (blue circle). The limb segments can freely rotate around the shoulder at  $\mathbf{0}$  and elbow at  $\mathbf{x}_e$  (red points in open circles). The hand at the end of the forearm,  $\mathbf{x}_h$ , should reach a target at  $\mathbf{x}_g$  (purple circle). The direct motion along the dashed purple curve leads to a collision with the obstacle and hence it is prohibited. B) The extended obstacle,  $E(\mathbf{x})$ , in the hand space  $\mathcal{H}$  is made up of the hand positions corresponding to contact of the forearm with the obstacle at different angles. The orange thick curve delimiting the extended obstacle corresponds to the hand positions given that the forearm slides around the obstacle.

Without loss of generality let us first assume that there exists a single point-like target at  $\mathbf{x}_g \in \mathcal{W}$  and an obstacle at  $\mathbf{x} \in \mathcal{W} \setminus \bar{\mathcal{B}}_{\rho}(\mathbf{0})$ , i.e., outside the circle area of radius  $\rho$  delimited by the upper arm (Fig. 1A, purple and blue circles, respectively). The forearm segment cannot cross the obstacle, which sets a constraint to the limb movement. In particular, the hand cannot directly reach the target (Fig. 1A, dashed purple trajectory is prohibited). Indeed, by extending the limb towards the target we end up in

a situation when the forearm touches the obstacle (Fig. 1B). Thus, at time  $t > 0$ ,  $\exists \lambda \in [0, 1]$  such that

$$\mathbf{x} = \lambda \mathbf{x}_h + (1 - \lambda) \mathbf{x}_e. \quad (1)$$

Therefore, to reach the target the limb first must bend going down and then extend to the target. The situation becomes much more complex if during the motor execution of the catching task the obstacle and/or target move in the plane  $(x_1, x_2)$  or in 3D space (see below).

## 2.2. Hand space

Let us remind that to enable the GCM concept, we have to eliminate the spatial dimensions and rotational degrees of freedom of the limb and represent it as a point in some 2D space equivalent to  $\mathcal{W}$ .

### 2.2.1. Compaction of forearm

We now introduce a *hand-space*  $\mathcal{H}$  isometric to the workspace, i.e.,  $\mathcal{H} = \bar{\mathcal{B}}_{\rho+1}(\mathbf{0}) = \mathcal{W}$ . All objects from the workspace are mapped into the hand-space. However, this mapping depends on the type of object.

In the case of the limb the mapping results in a compaction of the forearm:

$$\begin{aligned} C : \mathcal{P}(\mathcal{W}) &\rightarrow \mathcal{H} \\ I &\mapsto \mathbf{x}_h, \end{aligned} \quad (2)$$

where  $I \subset \mathcal{W}$  is the forearm segment (with ends  $\mathbf{x}_e$  and  $\mathbf{x}_h$ ). In other words, the forearm is reduced to a single point located at the hand position  $\mathbf{x}_h \in \mathcal{H}$ .

### 2.2.2. Extension of point-like obstacles

Given the desired mapping of the forearm into a point, the mapping of obstacles goes in an opposite way. A point obstacle in the workspace is mapped into a curve, i.e., we obtain an extended obstacle in the hand-space. Geometrically this extended obstacle is represented by all possible positions of the hand corresponding to contact of the forearm with the obstacle in the workspace (Fig. 1B).

For further calculations we assume that the obstacle is reachable by the forearm only. Then

$$\mathbf{x} \in \mathcal{A} = \bar{\mathcal{B}}_{\rho+1}(\mathbf{0}) \setminus \mathcal{B}_\rho(\mathbf{0}), \quad (3)$$

where  $\mathcal{A} \subset \mathcal{W}$  is the annulus containing the obstacle. In other words, the upper arm cannot contact the obstacle. We then define a local coordinate system  $(\bar{x}_1, \bar{x}_2)$  (Fig. 1A, green), rotated by angle  $\theta$  in such a way that the axis  $\bar{x}_1$  points to the obstacle. Denoting by  $\phi$  the angle that the upper arm forms with  $\bar{x}_1$ -axis (Fig. 1A), we express the distance between the elbow and the obstacle as a function  $\lambda_{\mathbf{x}} : [-\phi_{\max}(\mathbf{x}), 0] \rightarrow [|\|\mathbf{x}\| - \rho, 1]$ :

$$\lambda_{\mathbf{x}}(\phi) = \|\bar{\mathbf{x}}_e(\phi) + \bar{\mathbf{x}}\| = (\rho^2 + \|\mathbf{x}\|^2 - 2\rho\|\mathbf{x}\|\cos\phi)^{\frac{1}{2}}, \quad (4)$$

where  $\bar{\mathbf{x}}_e(\phi) = r(\cos\phi, \sin\phi)^T$  and  $\bar{\mathbf{x}}$  represent the elbow and obstacle positions in the new reference, respectively. Note that if the forearm contacts the obstacle, then  $\phi < 0$  and  $h_{\mathbf{x}}(\phi) \leq 1$ . Thus, taking

$$\phi_{\max}(\mathbf{x}) = \arccos\left(\frac{\rho^2 + \|\mathbf{x}\|^2 - 1}{2\rho\|\mathbf{x}\|}\right), \quad (5)$$

we can restrict the study to the case  $\phi \in [-\phi_{\max}(\mathbf{x}), 0]$ .

We can now generalize Eq. (1) and express the relation between the positions of the obstacle, the elbow, and the hand as:

$$\bar{\mathbf{x}}_h(\phi) = \frac{\bar{\mathbf{x}}}{\lambda_{\mathbf{x}}(\phi)} - \left[\frac{1}{\lambda_{\mathbf{x}}(\phi)} - 1\right] \bar{\mathbf{x}}_e(\phi). \quad (6)$$

Note that Eq. (6) contains a free parameter  $\phi$  and thus it generates a set of hand positions corresponding to contact of different parts of the forearm with the obstacle (Fig. 1B).

Now taking into account that the rotation between the local and original axes is given by the matrix

$$\mathcal{M}(\mathbf{x}) = \frac{1}{\|\mathbf{x}\|} \begin{pmatrix} x_1 & -x_2 \\ x_2 & x_1 \end{pmatrix}, \quad (7)$$

where  $\mathbf{x} = (x_1, x_2)^T$ , it remains only to undo the change of variables:  $\mathbf{x}_h = \mathcal{M}\bar{\mathbf{x}}_h$ . Thus, under the mapping  $F : [-\pi, \pi] \times \mathcal{A} \rightarrow \mathcal{H}$ , defined in the original coordinates by

$$F(\phi, \mathbf{x}) = \frac{\mathbf{x}}{\lambda_{\mathbf{x}}(\phi)} - \rho \left[ \frac{1}{\lambda_{\mathbf{x}}(\phi)} - 1 \right] \mathcal{M}(\mathbf{x}) \begin{pmatrix} \cos \phi \\ \sin \phi \end{pmatrix}, \quad (8)$$

a point-like obstacle  $\mathbf{x} \in \mathcal{A} \subset \mathcal{W}$  in the workspace is mapped into a spatially extended obstacle  $E(\mathbf{x}) \subset \mathcal{H}$  in the hand space. Finally, the map transforming obstacles from the workspace to the hand-space is given by  $E : \mathcal{A} \rightarrow \mathcal{P}(\mathcal{H})$

$$E(\mathbf{x}) = \{F(\phi, \mathbf{x}) : \phi \in [-\phi_{\max}, 0]\} \quad (9)$$

We remark that the set  $E$  depends on the position of the obstacle, but not on the position of the hand. We will use this property later when dealing with modeling the movement of the hand. We also note that the obstacle position in the workspace is mapped to the same position in the hand-space. Indeed,  $\lambda_{\mathbf{x}}(-\phi_{\max}(\mathbf{x})) = 1$  and hence  $F(-\phi_{\max}(\mathbf{x}), \mathbf{x}) = \mathbf{x}$ .

To finish the object mapping between the work- and hand-spaces we add that targets (could be many) are mapped with no change to the hand-space. This means that we aim at catching a target by the hand and not simply touching it by the forearm.

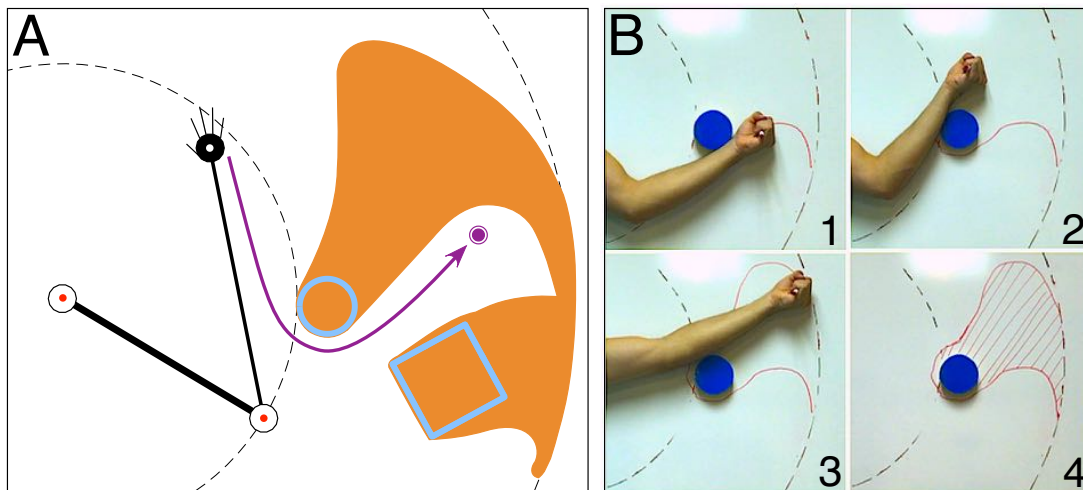


FIGURE 2. Examples of extended obstacles in the hand space. A) Numerical simulation. Two obstacles in the workspace with circular and square shapes are shown in blue. The corresponding extended obstacles in the hand-space are shown in orange. The purple curve represents a feasible trajectory to the target. Dashed black circles delimit the annulus  $\mathcal{A}$ . B) Generation of an extended obstacle by a human (three consecutive snapshots and the final extended obstacle are shown in panels 1–4). The hand moves continuously ensuring that the forearm always touches the static obstacle (blue cylinder) attached to a whiteboard. Along the movement the curve drawn by a marker depicts the boundary of the extended obstacle.

Thus, the above described mapping enables compacting the limb into a point (by applying the compaction  $C$ ), but at the same time it extends point obstacles into closed bounded sets (by applying the extension  $E$ ). Then a real obstacle with non-zero dimension can be mapped from the workspace to the hand-space by applying the transformation (9) to the obstacle boundary. Figure 2 illustrates two examples of the obstacle mapping. In the first case we use a circular and square shape obstacles and draw their images in the hand-space (Fig. 2A, orange area). Note that in the hand-space obstacles can overlap thus forming one big obstacle. In the second case we illustrate how the extended obstacle can be drawn by a human. The shoulder was fixed in space and the person was asked to move his left arm in such a way that the forearm would always keep contact with the obstacle (Fig. 2B, blue cylinder). The resulting extended obstacle (Fig. 2B, shaded in red) is similar to that obtained in the simulation (compare to the circle in Fig. 2A).

We remark that the concept of extended obstacles is closely related to the reachability set used in control theory (see, e.g., [20, 21]). Such a set is defined by feasible trajectories generated by a dynamical system, i.e., without collisions, fulfilling the desired task and system constraints. In this context, the initial reachable set for the manipulator shown in Fig. 2A is an annulus of a proper radius. Then in the presence of obstacles the set is restricted to those limb-trajectories that avoid hand penetration into the region occupied by the extended obstacles (shown in orange).

### 2.3. Generalized cognitive maps in hand-space

Let us now consider a manipulator actuating in a dynamic situation. Then obstacles and/or targets can move in the workspace. To actuate the manipulator we will employ generalized cognitive maps. However, the GCM concept cannot be applied directly in the workspace. Instead, we will construct GCMs in the hand-space where the manipulator is reduced to a point-like object.

To build a GCM we simultaneously model two main elements (see [15] for more details): i) movement of obstacles and ii) matching the obstacle movement with all possible subject actions. Note that both calculations are performed “mentally” in a neural network and must be done faster than the time scale of the dynamic situation (for more detail see [17]). Thus, in what follows we will deal with two times: i)  $t$  is the “real” time in the workspace, and ii)  $\tau$  is the “mental” time used in mental calculations made by a neural network. Then a trajectory  $\mathbf{x}_h(\tau)$  obtained in the hand-space can be implemented in the workspace simply by rescaling time  $\tau$ . In Sect. 3.3 we provide an experimental verification of the results using a robot NAO (Aldebaran Robotics). Therefore, we have adapted the calculations to the robot and obtained the scaling constant  $\kappa = t/\tau = 1/400$  [s].

#### 2.3.1. Obstacle movements in hand-space

The first ingredient of a GCM is the transformation to the hand-space described in Sect. 2.2. Under this transformation the arm is mapped into a point coinciding with the initial location of the hand in the workspace, while the obstacles are extended into bigger objects (Fig. 2).

To predict the trajectories of objects in the workspace earlier we used a recurrent neural network that approximated trajectories by Taylor series up to quadratic terms [15, 18]. The Taylor coefficients were estimated by the network from the initial conditions provided by the sensory system of the subject. Here we use a similar but purely computational approach. The trajectories are predicted using the initial (at  $t = 0$ ) velocities and accelerations and taking into account physical constraints.

The displacement of an obstacle in the workspace (with time  $t$ ) implies not only the movement of the corresponding extended obstacle in the hand-space (with time  $\tau$ ), but also a time-dependent adjustment of its shape. Indeed, the extended obstacle, Eq. (9), depends nonlinearly on the obstacle position in the workspace,  $\mathbf{x}(t)$ . Thus, for each instant of the mental time  $\tau$  we predict the future obstacle position in the workplace and then evaluate its representation in the hand-space by applying transformation (9) to points in the obstacle boundary. Figure 3 shows an example of how two objects moving in the workspace can be projected into the hand-space. Note the changes in the shape of the extended objects.

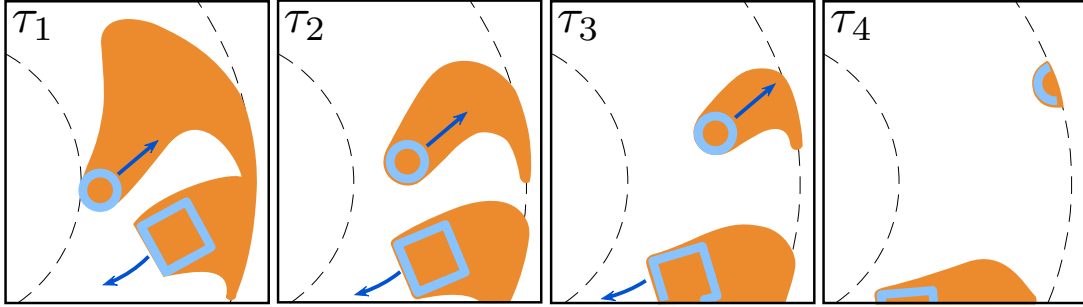


FIGURE 3. Prediction of movements of two obstacles in the workspace (in blue) and their mapping into the hand-space (orange areas). Blue arrows mark the directions of obstacle movements. Note changes in the shape of the extended obstacles at different time instants  $\tau_{1-4}$ .

### 2.3.2. Matching obstacle movements with subject actions by causal neural network

We simulate all possible hand movements in the hand-space and match them with extended objects in a 2D neuronal lattice. The lattice is composed of  $80 \times 80$  locally coupled FitzHugh-Nagumo-type neurons described by the following dynamical system

$$\begin{aligned} \frac{dr_{ij}}{d\tau} &= q_{ij} (f(r_{ij}) - z_{ij} + d\Delta r_{ij}) \\ \frac{dz_{ij}}{d\tau} &= \varepsilon (r_{ij} - 7z_{ij} - 2) \end{aligned} \quad (i, j) \in \Lambda, \quad (10)$$

where  $\Lambda = \{(i, j) \in \mathbb{N}^2 : 1 \leq i, j \leq 80\}$  is the network space;  $r_{ij}$  and  $z_{ij}$  are the membrane potential and recovering variable of neuron  $(i, j)$ , respectively;  $\Delta$  is the discrete 2D Laplacian;  $f(r) = (-r^3 + 4r^2 - 2r - 2)/7$  is the typical nonlinearity. In numerical experiments we set the diffusion constant to  $d = 0.2$  and the small parameter to  $\varepsilon = 0.04$ . The selected functions and parameter values in (10) ensure propagation of a phase wave in the lattice. The system is considered with Neumann boundary conditions. The function  $q_{ij}(\tau)$  describes effective objects and will be discussed in Sect. 2.3.3.

At the beginning all neurons except one stay at rest ( $r_{ij}(0) = z_{ij}(0) = 0$ ). The neuron  $(i_h, j_h)$  corresponding to the hand location has no dynamics  $q_{i_h, j_h} = 0$  and hence  $r_{i_h, j_h}(\tau > 0) = r_{i_h, j_h}(0) = 5$ . This cell will initiate a phase wave in the lattice. Such a wave simulates all possible movements of the hand in a single run. Points on the wavefront at time instant  $\tau^*$  describe all positions virtually available to the hand. Then the wave explores the environment and finds ways to the target if they exist (for more details see [15, 18]).

To illustrate the idea let us consider a situation similar to that shown in Fig. 1A, but now the point-like obstacle moves in certain direction (Fig. 4A, blue arrow). In the hand space the arm is mapped into a point while the obstacle is extended to a curve (Fig. 4B). The displacement of the obstacle for  $\tau > 0$  implies changes in its shape (see also Fig. 3).

### 2.3.3. Phase wave generates effective objects and builds generalized cognitive map

At  $\tau > 0$  a wavefront propagates in the lattice and switches cells to upstate (Fig. 4C). The time instant  $\tau = c$  when cell  $(i, j)$  crosses a threshold (i.e.,  $r_{ij}(c) = r_{th}$ ) is stored. Thus, behind the wavefront we obtained a potential field  $\{c_{ij}\}$ . The circular shape of the wavefront at the beginning (Fig. 4C,  $\tau = 30$  and  $\tau = 100$ ) means that the hand can move equally in all directions. Then at a given  $\tau^*$  it can occupy any place on the circle corresponding to the wavefront. However, this circular shape is broken once the wave starts interacting with objects (obstacles and target). Such events correspond to possible collisions of the hand with obstacles or the target. The formers should be avoided, whereas the latter is desired (i.e., the hand touches the target in mental simulation).

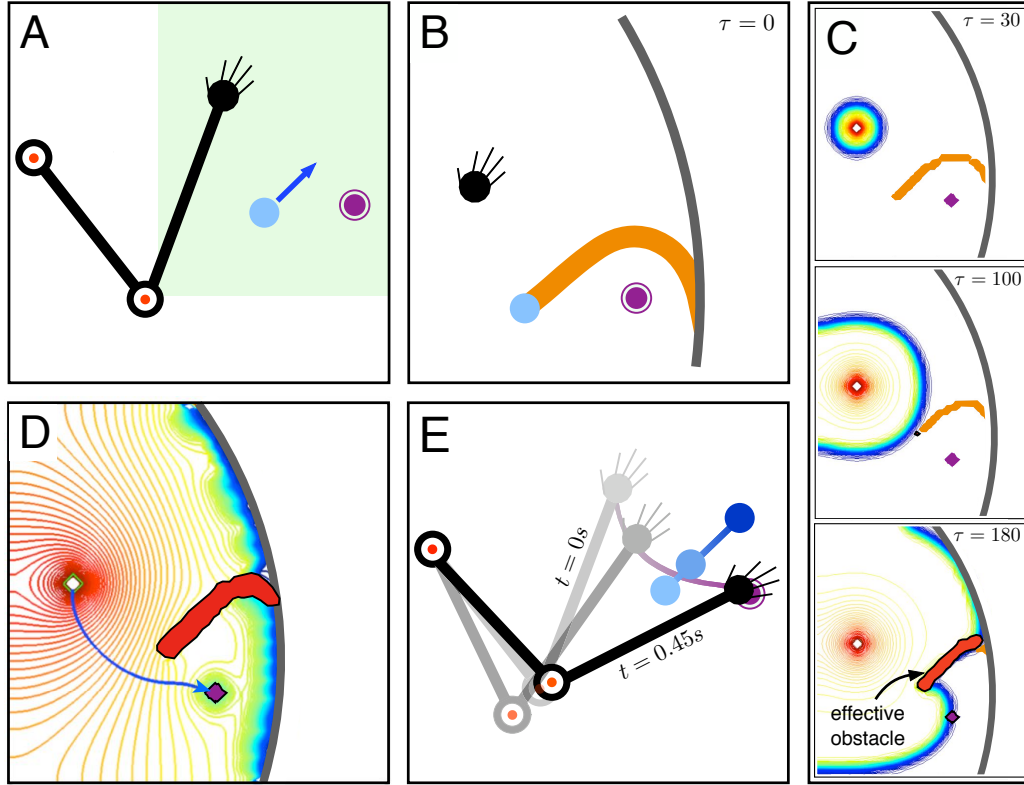


FIGURE 4. Generalized cognitive map controlling the movement of a limb in a simple dynamic situation. A) Initial situation similar to Fig. 1A, but the obstacle (blue circle) moves along the direction shown by blue arrow. The hand should reach the target (purple circle) and avoid collision with the obstacle. Shaded by green region is used in other subplots. B) The situation in the hand-space. The limb is reduced to a point (black circle) while the extended obstacle for  $\tau = 0$  is shown in orange. C) The process of generation of a generalized cognitive map. Snapshots illustrate the traveling wavefront exploring the environment. D) The generalized cognitive map of the situation. The static effective obstacle is shown in red. Blue arrowed curve marks the shortest feasible path to the target obtained by the gradient descend method. E) Superimposed snapshots of the limb movement in the workspace (darker colors correspond to progressively increasing time instants). At the end the hand successfully reaches the obstacle.

For further numerical simulations it is convenient to introduce the discrete mental time  $k = 0, 1, \dots$  that relates to the continuous time by  $\tau = k\Delta$ , where  $\Delta$  is the integration time step. Then we denote by  $\Gamma(k)$  the set of cells  $\{(i, j)\} \in \Lambda$  occupied by the obstacles and targets at time instant  $k$ . We also define the following iterative process:

$$\begin{aligned} \Omega(0) &= \emptyset \\ \Omega(k) &= \Omega(k-1) \cup \delta\Omega(k), \quad k = 1, 2, \dots \end{aligned} \quad (11)$$

where  $\delta\Omega(k) = \{(i, j) \in \Lambda : r_{ij}(k\Delta) \in [1, 2], (i, j) \in \Gamma(k)\}$ . The set  $\Omega(k)$  describes effective objects in the network space  $\Lambda$ . It is dynamically created as the wavefront explores  $\Lambda$ . The set grows (i.e.,  $\delta\Omega(k) \neq \emptyset$ ) if the wavefront touches an object at  $\tau = k\Delta$ . Then we define the function  $q : (0, \tau_{\max}) \times \Lambda \rightarrow \{0, 1\}$  used in Eq. (10):

$$q_{ij}(\tau) = \begin{cases} 0, & \text{if } (i, j) \in \Omega(k) \\ 1, & \text{otherwise} \end{cases}$$

The cells in  $\Omega(k)$  have  $dr/d\tau = 0$  for  $\tau > k\Delta$  and hence will exhibit no dynamics, i.e., the effective objects are *static* and the wavefront slips around them (Fig. 4C,  $\tau = 180$ ).

We note that although  $\Lambda$  is a square lattice, only exploration of the part corresponding to the annulus  $\mathcal{A}$  is of interest. The hand cannot reach locations outside the disk  $\bar{\mathcal{B}}_{\rho+1}$ . Thus, we can artificially add an obstacle at  $\delta\mathcal{B}_{\rho+1}$ , which will restrict the wave propagation (Fig. 4C, black circle-like curve). Once the wave exploration of  $\Lambda$  has been finished, the created potential field  $G = (c_{ij}) \in \mathcal{M}_{80 \times 80}$  represents a generalized cognitive map of the situation (Fig. 4D). It contains spatiotemporal relationships among the hand and other objects in the workspace structured as static effective objects in the hand-space. These effective objects contain critical information about possible collisions of the arm and obstacles (to be avoided) and the target (to be caught).

### 2.3.4. Motor execution of movement in workspace

The GCM concept developed above allows representing a dynamic situation as a static map in the hand-space (Fig. 4D):

$$G = G(\mathbf{y}) \quad \mathbf{y} \in \Lambda \quad (12)$$

All objects (targets and obstacles) including moving ones are replaced by the corresponding static effective objects. The gradient profile,  $\nabla_{\mathbf{y}}G$ , imposes rules the hand should follow to reach the target. We thus use a gradient descend method to find trajectories connecting the hand and the target positions (Fig. 4D, blue arrowed curve). By construction such a trajectory circumvents effective obstacles in the hand-space. However, what is more important, if the hand follows this trajectory in the workspace then:

- The hand will reach the target;
- During the move the limb will not bump against obstacles.

Therefore, in order to solve the dynamical situation in the workspace we use the trajectory obtained in the hand-space and implement kinematic movements of the limb in such a way that the hand would follow this trajectory. Figure 4E shows three superimposed snapshots of the moving manipulator and obstacle in the workspace. The manipulator successfully accomplishes the task: “reach the target and avoid collisions with obstacles”, as expected.

The proposed approach builds a basis for cognitive manipulators working in time-evolving situations. Note that a rather simple situation represented in Fig. 4 has been used for illustration purpose only. The concept applies to situations of arbitrary complexity up to the granularity of the neural network.

## 3. Cognitive limb movement in 3D

Cognitive manipulation in three-dimensional space can be straightforwardly tackled by the GCM concept described in Sect. 2. However, it implies constructing extended obstacles and simulating phase waves in 3D space, which requires significantly higher computational resources. Nonetheless, a simpler approach to 3D dynamic situations can be applied.

### 3.1. Reduction of 3D problem to 2D plane

Figure 5A shows an example of a manipulator in 3D space. The limb should catch a ball falling due to the gravity force and avoid collision with a fixed horizontal bar. We then can assume that the limb movements are restricted to plane  $P$  formed by the upper arm and forearm. Then the 3D problem is reduced to considering a two-joint manipulator on a plane with 2D objects obtained by intersecting 3D objects (the ball and the bar) with the plane (Fig. 5B). Note that the latter problem is equivalent to the problem shown in Fig. 4, but now the target is mobile and the limb should intercept it. Thus, we can apply directly the procedure described in Sect. 2.

In the 2D projection the static obstacle (blue bar) and the moving target (purple ball) are represented by the corresponding disks. Since the obstacle is static its representation in the hand-space will be also static (Fig. 5C, orange area). As we discussed above the target is not extended in the hand-space (Fig.

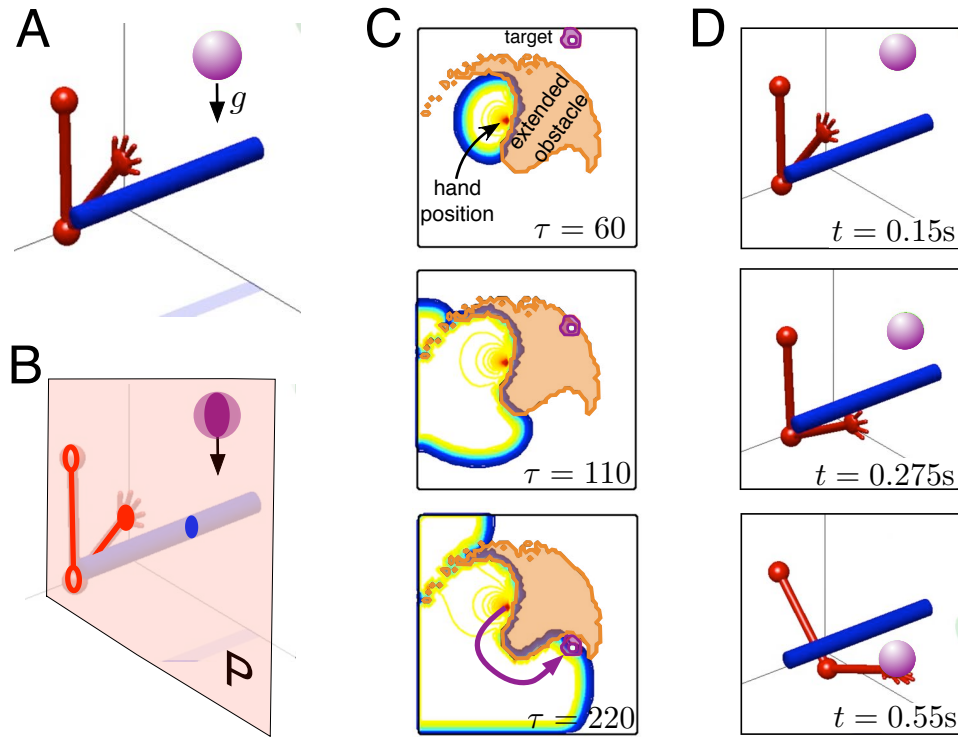


FIGURE 5. Catching a falling ball: Reduction of the cognitive manipulation in 3D space to a quasi 2D problem. A) A limb (in red) catches a ball (in purple) falling due to the gravity force. The horizontal bar (in blue) is a fixed obstacle. B) Given that the limb moves in plane  $P$  the problem is reduced to 2D. C) Snapshots of the wave generating a generalized cognitive map in mental time  $\tau$ . The static extended obstacle is drawn in orange. The moving target is in purple. Note that the target is not extended in the hand space. Purple arrowed curve marks the hand trajectory to intercept the falling ball. D) Simulation of the limb movement in real time  $t$ .

5C, purple disk). Then the wave process similar to that shown in Fig. 4 starts. The wave propagates from the hand position outwards and matches all possible hand movements with the target motion. We search for a contact of the wave with the target, which occurs at mental time  $\tau = 220$  (Fig. 5C).

Once a contact of the wave with the target has been achieved we can stop the calculation and draw a curve from the hand position to the place of contact following the gradient of the field  $G(\mathbf{y})$  (Fig. 5C, panel  $\tau = 220$ , arrowed curve). Now this trajectory can be implemented by the limb in real time  $t$ . Figure 5D shows snapshots of the manipulator movements in the workspace and real time  $t$ .

### 3.2. Selective catching of thrown objects

In order to illustrate how the GCM-based manipulation can cope with complex dynamic situations we consider a computational experiment in which the virtual arm must catch a moving target and avoid bumping into another moving obstacle.

Figure 6A sketches the situation. Imagine that two objects: a spinning bar (target, colored in purple) and a spinning disk (obstacle, colored in blue) where thrown and at some time instant  $t$  cross simultaneously the arm plane  $P$  in opposite directions. The arm should catch the bar.

To solve the problem, we map the situation developing in the plane  $P$  into the hand-space and use the wave dynamics to match the hand movement with the object movements. Figure 6B shows consecutive

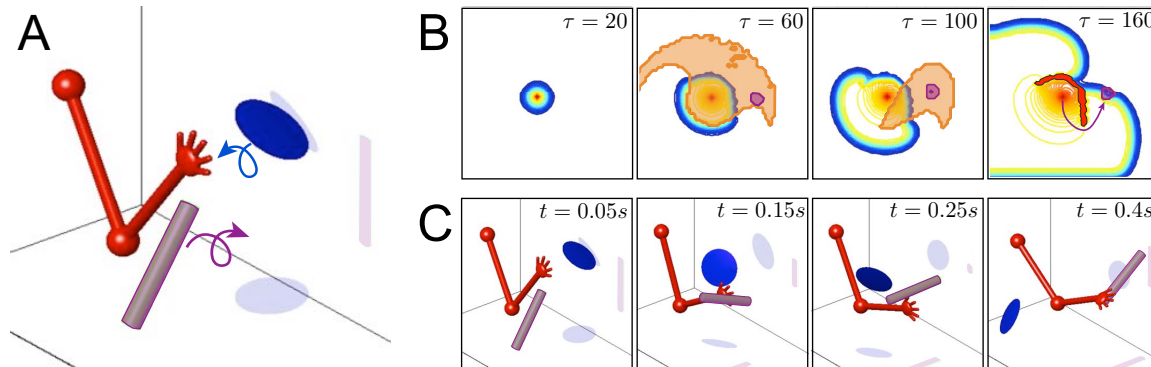


FIGURE 6. Selective catching of thrown objects. A) Sketch of the situation. A bar (target, purple) and a disk (obstacle, blue) move perpendicular to the arm plane (containing the arm). On the fly the objects spin around themselves, which leads to different intersections with the arm plane. B) Snapshots of the process of generation of the generalized cognitive map. The wavefront propagates and interacts with the extended obstacle (in orange) and with the target (in purple) [panels  $\tau = 20, 60$ , and  $100$ ]. Once the front touches the target (panel  $\tau = 160$ ), we get a trajectory (purple arrowed curve) that ensures collision-free target catching. C) Simulation of the arm movement in workspace. The hand catches the bar with no collision with the disk by following the trajectory provided by the GCM.

frames of the GCM generation. At  $\tau = 20$  neither the bar nor the disk crosses the plane  $P$  hence there is no objects in the hand-space and the wave has a circular shape. At  $\tau = 60$  and  $100$  both objects intersect the arm plane and we have them in the hand-space. Note that the extended obstacle (orange image of the disk in the hand-space) occupies large space in front and behind the wavefront. According to the causality principle the part of the extended obstacle that appears behind the wavefront does not change the virtual past (for more detail see [15]). Thus, the wave interacts only with the part of the obstacle that contacts the wavefront. Then this portion of the wavefront is “frozen” (i.e., the corresponding  $\{q_{ij}\}$  are set to zero in Eq. (10)). Finally, at  $\tau = 160$  the wavefront touches the target and we can draw a trajectory connecting the hand position with the the effective target.

Figure 6C illustrates the movement of the virtual arm coordinated with the movements of the bar and disk. The hand follows the trajectory found in the generalized cognitive map and, consequently, it avoids collision with the disk and catches the bar, as expected.

### 3.3. Experimental verification mimicking human ability

Humans in the childhood develop impressive sensory-motor skills including the ability of catching moving objects in the presence of obstacles. In the final experiment we provide a verification of the theory in a situation where a human and a robot have to perform the same cognitive task of catching a moving object and simultaneously avoiding collision with an obstacle.

We then prepared a setup consisting of a box made of cardboard (size  $h \times l \times w = 26 \times 60 \times 38$  cm) and a tennis ball attached to a cord. The other end of the cord was fixed at  $h = 150$  cm thus we get a pendulum like device. The box was considered as a static obstacle, whereas the ball was a target. We implemented movements of an artificial manipulator by using the right arm of a humanoid robot NAO. The robot is relatively small (height 57 cm, length of the arm 27 cm), thus as a human subject we used a ten-year-old boy. Figure 7 shows the experimental situation with the boy (panel A), in numerical simulation (panel B), and with the robot (panel C). The motor ability of the robot are much modest than those of a human. It takes around 200 ms to perform a simple enough motor pattern. Thus, we adjusted the cord length and the initial position of the ball in such a way that it would be reasonable to catch it by the robot.

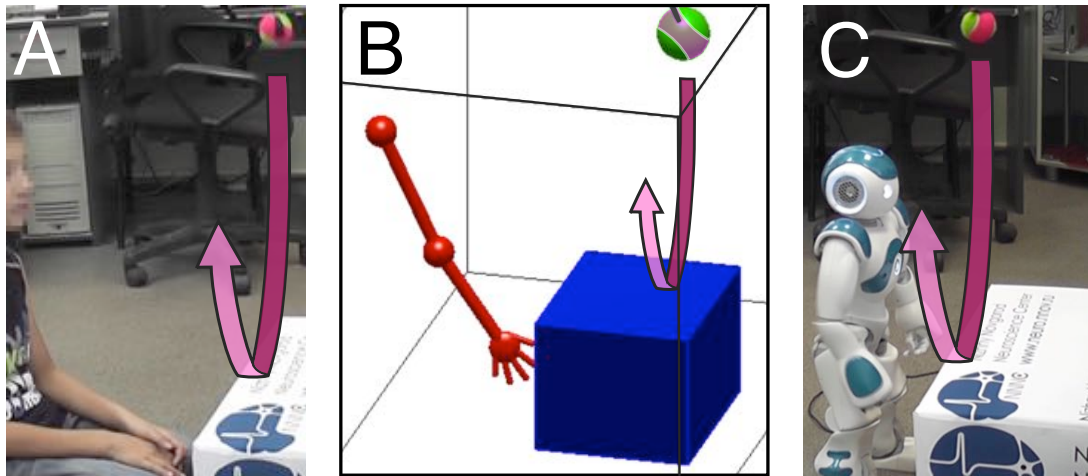


FIGURE 7. Experimental verification of the GCM theory: A pendulum experiment. A) A boy should reach by his right arm an oscillating tennis ball attached to a cord. Initial situation is shown. The ball starts going down towards the observer (red arrow). B) The same situation but in computer simulation. The GCM model solves the problem and provides a trajectory for the arm movement. C) Humanoid robot NAO mimics the human cognitive process of catching the ball by implementing the trajectory provided in the simulation.

Figure 8 summarizes the experimental results. First we performed the experiment with the boy. Figure 8A shows three snapshots of the catching process. The boy successfully accomplished the task. Then we performed the same task with the robot. At the beginning the situation was modeled in the neural network. Figure 8B illustrates the process of wave exploration of the environment. The static obstacle (cardboard box) has a static image in the hand-space (orange area in panel  $\tau = 0$ ). The wave bends it (panel  $\tau = 120$ ) and then in the hand-space there appear the ball (purple disk in panel  $\tau = 280$ ) and another extended obstacle corresponding to the cord (orange area in the top-right corner). The wavefront reaches the target and thus we get a generalized cognitive map of the situation (panel  $\tau = 280$ ). Purple arrowed curve marks the shortest feasible trajectory to the target. The obtained solution can be cross-checked by simulating the scenario (Fig. 8C). Finally, Fig. 8D shows the experimental implementation of the robotic arm movement. The arm follows the trajectory provided by the simulation and the robot hand catches the ball. Thus, this experiment confirms the suitability of the GCM-based arm movement for real robots.

#### 4. Discussion

The fundamental bases of how our brain solves different tasks of cognitive object manipulation, such as catching a moving ball in the presence of obstacles, remain largely unknown. Advances in this direction may significantly improve the motor skills of modern humanoid robots. In this work we have proposed a novel approach that allows solving the problem of an efficient limb movement in dynamic situations on an abstract cognitive level. We have validated our approach by numerical simulations and experimentally by using a humanoid robot NAO.

The approach relies on two main ingredients: i) Transformation of the problem from the limb workspace to the hand-space, and ii) Construction of a generalized cognitive map in the hand-space. A GCM naturally enables tracing a trajectory to a target that, in general, can be mobile. Then, due to specific properties of the hand-space this trajectory can be followed by the limb, which ensures a collision-free movement and target catching in the workspace.

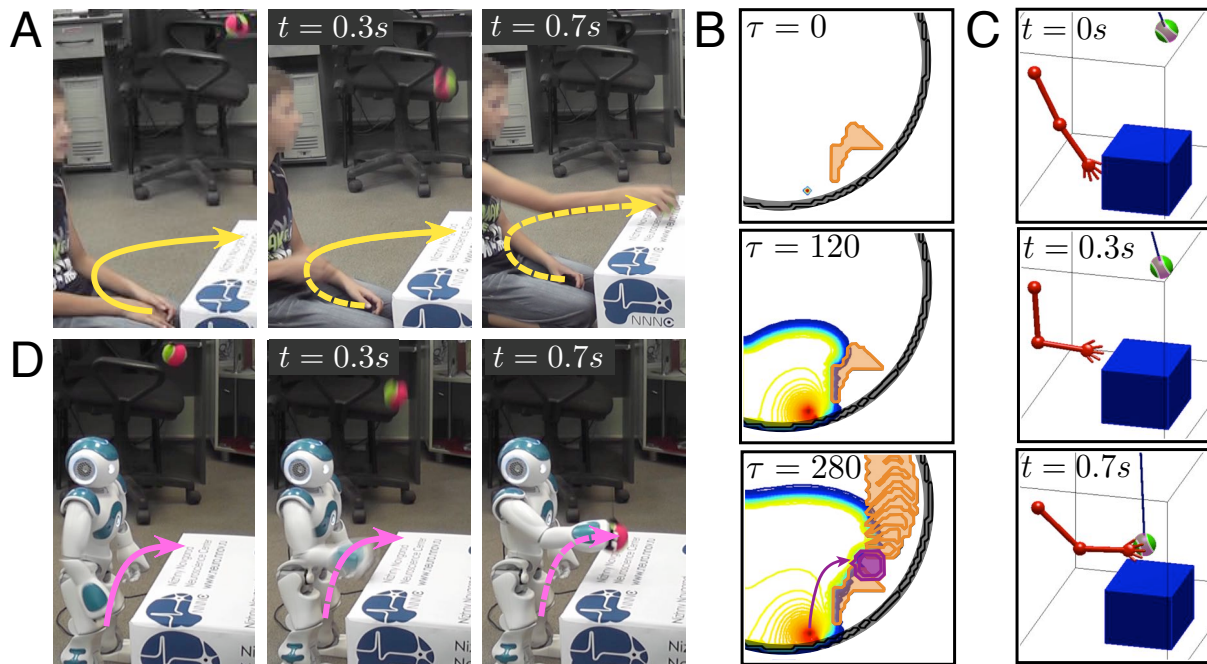


FIGURE 8. Mimicking a human cognitive ability by a robot equipped with generalized cognitive maps. A) The human solution to the problem presented in Fig. 7 . B) The process of generation of the generalized cognitive map. The static obstacle (cardboard box) is mapped into a static extended obstacle (orange, panel  $\tau = 0$ ). The wave bends the obstacle and finds all possible hand trajectories (panel  $\tau = 120$ ). When the ball crosses the arm plane in the hand space there appear the target (purple disk) and an extra extended obstacle corresponding to the cord (panel  $\tau = 280$ ). C) Simulation of the robot arm movement. D) Implementation of the process of catching the ball by the robot. The robot arm follows the trajectory provided by the simulation and catches the ball.

Traditional cognitive maps serve for navigation and path planning in complex but static scenarios. The GCM theory generalizes cognitive maps into description of dynamic situations [15]. A wave process taking place in a neural network explores “mentally” the agent’s environment and matches possible agent movements with those of the environment. It allows converting a dynamic situation into a static map. In certain sense it is similar to reducing a movie to a single picture. The resulting GCM contains both the information required to *understand* the situation and that needed to *interact* with it.

Since GCMs assume no internal degrees of freedom in the agent, they cannot be applied immediately to limbs. To remedy this problem we have considered the hand as the most relevant part of the limb that interacts with the environment. Then the hand positions such that the forearm touches obstacles delimit the so-called “extended” obstacles. In this context, the extended obstacles are related to the reachability set widely used in control theory [20]. We thus introduced a hand-space as a specific version of the configuration spaces commonly used for the limb description [19]. However, instead of using the standard approach employing joint angles, we constructed the hand-space isometric to the workspace. In the hand-space the arm is reduced to a point, which enables GCMs. Note that the complexity of extended obstacles in the hand space plays no role for building a GCM (although it may affect the existence of trajectories to the target). Finally, a trajectory of the hand movement provided by the GCM guarantees a collision-free movement of the limb in the workspace.

In order to demonstrate the feasibility of the proposed approach we have performed numerical simulations. First we have illustrated how the arm catches a target in two-dimensional plane with a moving obstacle. Then we have shown that such a situation can be extended into more realistic scenarios in three-dimensional space. In this case we assumed that the limb moves in its natural plane formed by the upper arm and forearm. Our results have shown that the limb can avoid collisions with static and dynamic obstacles and catch mobile targets.

The numerical simulations confirmed success of the GCM-based solutions but also revealed the problem complexity. We then performed the pendulum experiment to explore the reproducibility of GCM solutions in real robots and compared them with the human behavior. The results validated the feasibility of our approach in real-life scenarios. The trajectories of the limb movement adopted by the human and the robot were similar, although the boy made a more pronounced curve. This happened due to a significant difference in size and movement velocity between the boy and the robot. Such an advantage allows the human selecting a safer but longer trajectory to the target.

We remark that despite the apparent simplicity of the pendulum experiment, in several occasions the boy failed to catch the ball. This shows that even simple dynamic situations can puzzle our brain. An accurate and fast limb movement in complex situations, e.g., during sport games, requires intensive training. In this regard we can distinguish two types of scenarios dealing with: i) static situations (e.g., dancing or playing piano) and ii) dynamic situations (e.g., playing basketball or martial arts). In both cases mastering the movement aims at automatizing the body behavior. This can be considered somehow straightforward in static scenarios. However, imaging how it is possible in dynamic situations is intriguing. Indeed, the terms “cognitive” and “automatic” could seem contradictory. Despite that, the GCM theory provides a functional framework for their unification and automation of limb movements in dynamic situations.

The GCMs maintain the main attribute of traditional cognitive maps: codification of “geographical” information and trajectories. However, they go a step beyond. They transform dynamic situations into static representations. In other words, static and dynamic situations may have the same static representation in our brain. Since GCMs are points in a proper hyperspace, the process of acting in time-changing situations can be naturally learned and memorized [18]. Thus, we erase the contradiction between cognitive and automatic actions, and open a way to automation of sophisticated behaviors. Moreover, the GCM theory enables classification of complex dynamic situations into well-structured sets of memories and experiences by means of standard methods of data clustering and machine learning. Therefore, it provides a functional bridge between *effective* cognition, dealing with direct interaction with the environment, and *abstract* cognition, whose impact over subject’s behavior is less immediate but much more profound.

*Acknowledgements.* The authors thank Prof. G. Osipov for providing access to experiments with robot NAO. This work was supported by the Spanish Ministry of Economy and Competitiveness under grant FIS2014-57090-P (theoretical development) and by the Russian Science Foundation under project 15-12-10018 (experimental verification in robot).

## References

- [1] D.M. Wolpert, Z. Ghahramani, M.I. Jordan. *An internal model for sensorimotor integration*. Science, 269 (1995), 1880-1882.
- [2] P. Dean, J. Porrill, C.F. Ekerot, H. Jorntell. *The cerebellar microcircuit as an adaptive filter: experimental and computational evidence*. Nat. Rev. Neurosci., 11 (2010), 30-43.
- [3] B. Schmidt, A.D. Redish. *Navigation with a cognitive map*. Nature, 497 (2013), 42-43.
- [4] Y. Sandamirskaya, S.K.U. Zibner, S. Schneegans, G. Schoner. *Using Dynamic Field Theory to extend the embodiment stance toward higher cognition*. New Ideas in Psychol., 31 (2013), 322-339.
- [5] M. F. Land. *Do we have an internal model of the outside world?* Phil. Trans. R. Soc. B, 369 (2014), 20130045
- [6] B.W. Tatler, M.F. Land. *Vision and the representation of the surroundings in spatial memory*. Phil. Trans. R. Soc. B, 366 (2011), 596-610

- [7] L. Pisella, H. Grea, C. Tilikete, A. Vighetto, M. Desmurget, G. Rode, D. Boisson, Y. Rossetti. *An automatic pilot for the hand in human posterior parietal cortex: toward reinterpreting optic ataxia*. Nat. Neurosci., 3 (2000), 729-736.
- [8] T. Aflalo, S. Kellis, C. Klaes, B. Lee, Y. Shi, K. Pejsa, C. Liu. *Decoding motor imagery from the posterior parietal cortex of a tetraplegic human*. Science, 348 (2015), 906-910.
- [9] S. Lobov, N. Krilova, I. Kastalskiy, V. Kazantsev, V.A. Makarov. *A human-computer interface based on electromyography command-proportional control*. Proc. 4 Int. Congr. Neurotech., Electron. Inform., (2016).
- [10] H. Hoffmann, P. Pastor, D.H. Park, S. Schaal. *Biologically-inspired dynamical systems for movement generation: automatic real-time goal adaptation and obstacle avoidance*. ICRA’09. IEEE Int. Conf. Robotics and Automation, (2009), 2587-2592.
- [11] D.H. Park, H. Hoffmann, P. Pastor, S. Schaal. *Movement reproduction and obstacle avoidance with dynamic movement primitives and potential fields*. 8th IEEE-RAS Int. Conf. Humanoid Robots, (2008), 91-98.
- [12] O. Brock, O. Khatib, S. Viji. *Task-consistent obstacle avoidance and motion behavior for mobile manipulation*. Proc. ICRA’02. IEEE Int. Conf. Robotics and Automation, (2002), 388-393.
- [13] S.M. Khansari-Zadeh, A. Billard. *A dynamical system approach to realtime obstacle avoidance*. Autonomous Robots, 32 (4) (2012), 433-454.
- [14] S. Kim, A. Shukla, A. Billard. *Catching objects in flight*. IEEE Trans. on Robotics, 30 (5) (2014), 1049-1065.
- [15] J.A. Villacorta-Atienza, M.G. Velarde, V.A. Makarov. *Compact internal representation of dynamic situations: Neural network implementing the causality principle*. Biol. Cybern., 103 (2010), 285-297.
- [16] J.A. Villacorta-Atienza, C. Calvo, V.A. Makarov. *Prediction-for-CompAction: Navigation in social environments using generalized cognitive maps*. Biol. Cybern., 109 (3) (2015), 307-320.
- [17] C. Calvo, J.A. Villacorta-Atienza, V.I. Mironov, V. Gallego, V.A. Makarov. *Waves in isotropic totalistic cellular automata: Application to real-time robot navigation*. Adv. Complex Syst., 19 (4,5) (2016), 1650012-18.
- [18] J.A. Villacorta-Atienza, V.A. Makarov. *Neural network architecture for cognitive navigation in dynamic environments*. IEEE Tran. Neur. Netw. Learn. Syst., 24 (12) (2013), 2075-2087.
- [19] M.W. Spong, S. Hutchinson, M. Vidyasagar. Robot modeling and control. (Vol. 3, New York: Wiley, 2006).
- [20] C. Moussaoui, R. Abbou, J.J. Loiseau. *On bounds of input-output systems. Reachability set determination and polyhedral constraints verification*. IFAC Proc., 47 (3) (2014), 11012-11017.
- [21] R.E. Allen, A.A. Clark, J.A. Starek, M. Pavone. *A machine learning approach for real-time reachability analysis*. Proc. IEEE/RSJ Int. Conf. Intell. Robots Syst., (2014), 2202-2208.